

Article

Modification of the Mohr–Coulomb Criterion and Its Application in the Cracking of Ring-Stiffened Cylinders Made of Titanium Alloy

Xiangyu Yu ^{1,2,*}, Kewang Xu ^{1,2}, Qiang Xu ^{1,2}, Aifeng Zhang ^{1,2} and Hao Zhang ²

¹ Taihu Laboratory of Deepsea Technological Science, China Ship Scientific Research Center, Wuxi 214082, China

² State Key Laboratory of Deep-Sea Manned Vehicles, China Ship Scientific Research Center, Wuxi 214082, China

* Correspondence: 84xiangyu@163.com; Tel.: +86-510-85555702

Abstract: TC4 ELI alloy is widely used in the marine, medicine, and aviation fields. The failure performance of TC4 ELI alloy is significantly different from that of other metal materials, such as steels. In this paper, a modified Mohr–Coulomb criterion is calibrated based on several kinds of specimens under different stress states and a 3D geometric representation of a modified Mohr–Coulomb fracture locus for TC4 ELI is obtained based on these parameters. The effectiveness of the modified M-C criterion is studied by a ring-stiffened cylinder made of TC4 ELI. The ultimate strength of the cylinder obtained in the simulation with the modified M-C criterion is close to that obtained in an external pressure experiment, which shows that the modified M-C criterion is suitable for predicting failure in pressure hulls made of titanium alloy used in the deep-sea field.

Keywords: TC4 ELI; Mohr–Coulomb criterion; pressure hull; cracking; deep sea



Citation: Yu, X.; Xu, K.; Xu, Q.; Zhang, A.; Zhang, H. Modification of the Mohr–Coulomb Criterion and Its Application in the Cracking of Ring-Stiffened Cylinders Made of Titanium Alloy. *Processes* **2024**, *12*, 1732. <https://doi.org/10.3390/pr12081732>

Academic Editor: Ligang Zhang

Received: 24 July 2024

Revised: 14 August 2024

Accepted: 16 August 2024

Published: 17 August 2024



Copyright: © 2024 by the authors. Licensee MDPI, Basel, Switzerland. This article is an open access article distributed under the terms and conditions of the Creative Commons Attribution (CC BY) license (<https://creativecommons.org/licenses/by/4.0/>).

1. Introduction

Titanium alloys have been used widely in the aviation, aerospace, and oceanic fields because of their high specific strength, excellent corrosion resistance, good weldability, and high-temperature performance at just half of the weight of steels. Plastic forming is one of the main forming methods used to fabricate titanium alloy components due to its reduction in the cost of materials and enhancement of the performance of the products. However, titanium alloys are difficult to form because of their high deformation resistance, low ductility, and large anisotropy. With the increasing demand for the employment of titanium alloys in deep-sea equipment, predicting the fracture behavior and of TC4 ELI is becoming important for the design of pressure hulls.

So far, lots of models have been developed to predict the failure behaviors of metals. There are two categories of ductile fracture models, which are coupled fracture criteria and uncoupled fracture criteria. The main difference between these two categories is whether the influence of damage on the metal's strength and deformation is considered. Of the categories of coupled ductile fracture models, the most well-known family is the Gurson–Tvergaard–Needleman (GTN) ductile models, which micromechanically consider void nucleation, growth, and coalescence [1–3]. The GTN criteria family has been modified by many researchers to improve the description of damage accumulation when stress triaxiality is low [4–6]. Continuum Damage Mechanics (CDM) is another family of coupled damage models. This family of criteria describes material failure using a continuum mechanics framework, and has advantages because of its physical background. The original frame was proposed by Lemaitre and Chaboche [7–9], and improved by Brunig [10]. The coupled damage modes are time-consuming and require complicated calibrating procedures, which limit the application in simulations.

On the other hand, the uncoupled fracture criteria are easier to embed in simulations. This family of criteria is a phenomenological model which was originally based on the weighted measurements of accumulated plastic strain. The well-known criteria of this family were based on the initial works by McClintock [11], Cockcroft [12], Rice and Tracey [13], Brozzo [14], and Oyane [15], and further developed by Clift [16] and Ko [17]. To extend the application of the uncoupled fracture criteria in simulations, Bai and Wierzbicki [18,19] proposed the modified Mohr–Coulomb criterion to deal with varied loading conditions. Based on their works, Xue [20] considered the effect of the Lode angle and hydrostatic pressure on fracture evolution. Khan et al. [21] proposed a fracture model based on the Magnitude of Stress Vector and considered the influence of temperature and strain rate on the ductile fracture of TC4 alloy. Isik et al. [22] introduced a shear fracture forming limit line by applying the theory of plasticity to proportional strain loading paths, and developed a new experimental method to obtain the values at the onset of fracture. These improved fracture criteria are employed to predict the fracture behavior of metal sheets under different loading conditions, namely uni-axial tension, in-plane shear, plane strain tension, and equi-biaxial tension.

TC4 ELI alloys have been used to gradually manufacture key ocean engineering equipment, such as the pressure hulls used in deep-sea vessels. Thanks to the low toughness of TC4 ELI alloys, their fracture behavior is quite different from that of high-strength steels (see Figure 1).



Figure 1. Fracture behavior of (a) high-strength steel and (b) TC4 ELI.

In this paper, a series of tests for obtaining mechanical properties are conducted, and based on the testing data, the parameters of the modified M-C criterion are calibrated. The new criterion is employed in the ultimate strength prediction of a ring-stiffened cylinder made of TC4 ELI, and the result is compared with the experiments. The comparisons show that the new criterion suits the fracture behavior well.

2. Modified Mohr–Coulomb Criterion

The original Mohr–Coulomb fracture criterion was proposed for cracks in rock and soil mechanics and other brittle materials. This stress-based criterion is simple and physically sound. As mentioned by Bai [19], material ductility depends on both stress triaxiality and the Lode angle parameter, and in [18] they proved that these two parameters control the fracture of ductile metals. On the other hand, the ductile fracture criteria usually employ the equivalent strain to fracture as a measurement of material ductility. The stress–strain form of the fracture criterion is justifiable because the resolution of strains is much larger than stresses. In order to transform the M-C criterion to the space of $(\bar{\epsilon}_f, \eta, \bar{\theta})$, where $\bar{\epsilon}_f$ is the equivalent strain to fracture, η is the stress triaxiality, and $\bar{\theta}$ is the normalized Lode angle, proceedings were proposed by Bai [19].

The M-C criterion is as shown as Equation (1):

$$(\tau + c_1\sigma_n)_f = c_2 \quad (1)$$

where c_1 and c_2 are material constants. c_1 is referred to as a friction coefficient, and c_2 is shear resistance. The M-C criterion can be considered as an extension of the maximal shear stress criterion.

In order to transform the M-C criterion to the space of $(\bar{\varepsilon}_f, \eta, \bar{\theta})$, $\eta, \bar{\theta}$ should be introduced as follows.

The three invariants of a stress tensor $[\sigma]$ are defined by

$$p = -\sigma_m = -\frac{1}{3}(\sigma_1 + \sigma_2 + \sigma_3) \quad (2)$$

$$q = \bar{\sigma} = \sqrt{\frac{3}{2}[S] : [S]} = \sqrt{\frac{1}{2}[(\sigma_1 - \sigma_2)^2 + (\sigma_1 - \sigma_3)^2 + (\sigma_2 - \sigma_3)^2]} \quad (3)$$

$$r = \left(\frac{9}{2}[[S] \cdot [S] \cdot [S]]\right)^{\frac{1}{3}} = \left[\frac{27}{2}(\sigma_1 - \sigma_m)(\sigma_2 - \sigma_m)(\sigma_3 - \sigma_m)\right]^{1/3} \quad (4)$$

where $[S]$ is the deviatoric stress tensor, and σ_1, σ_2 , and σ_3 are principal stresses. The stress triaxiality η is defined by

$$\eta = \frac{-p}{q} = \frac{\sigma_m}{\bar{\sigma}} \quad (5)$$

The Lode angle θ is related to the normalized third invariant as follows:

$$\cos(3\theta) = \left(\frac{r}{q}\right)^3 \quad (6)$$

Furthermore, the Lode angle can be normalized by

$$\bar{\theta} = 1 - \frac{6\theta}{\pi} = 1 - \frac{2}{\pi} \arccos\left(\frac{r}{q}\right)^3 \quad (7)$$

After normalization, the range of $\bar{\theta}$ is $-1 \leq \bar{\theta} \leq 1$.

The principal stresses can be expressed in the form of σ_m, η, θ .

$$\begin{cases} \sigma_1 = \left[1 + \frac{1 \cos \theta}{3\eta}\right] \sigma_m \\ \sigma_2 = \left[1 + \frac{2 \cos\left(\frac{2}{3}\pi - \theta\right)}{3\eta}\right] \sigma_m \\ \sigma_3 = \left[1 + \frac{2 \cos\left(\frac{4}{3}\pi - \theta\right)}{3\eta}\right] \sigma_m \end{cases} \quad (8)$$

The M-C criterion can be expressed in terms of principal stresses:

$$\left(\sqrt{1 + c_1^2} + c_1\right)\sigma_1 - \left(\sqrt{1 + c_1^2} - c_1\right)\sigma_3 = 2c_2 \quad (9)$$

By substituting Equation (8) into Equation (9), the M-C criterion can be expressed in terms of $\bar{\sigma}, \eta$, and θ :

$$\bar{\sigma} = c_2 \left[\sqrt{\frac{1 + c_1^2}{3}} \cos\left(\frac{\pi}{6} - \theta\right) + c_1 \left(\eta + \frac{1}{3} \sin\left(\frac{\pi}{6} - \theta\right)\right) \right]^{-1} \quad (10)$$

Based on the power type flowing model (Equation (11)) and Von Mises yield criterion, the M-C criterion can be expressed in terms of $\bar{\varepsilon}_f, \eta, \bar{\theta}$, which is shown as Equation (12).

$$\bar{\sigma} = A\bar{\varepsilon}^n \quad (11)$$

$$\bar{\varepsilon}_f = \left\{ \frac{A}{c_2} \left[\sqrt{\frac{1+c_1^2}{3}} \cos\left(\frac{\bar{\theta}\pi}{6}\right) + c_1 \left(\eta + \frac{1}{3} \sin\left(\frac{\bar{\theta}\pi}{6}\right) \right) \right] \right\}^{-\frac{1}{n}} \quad (12)$$

where A and n are the material parameters which can be determined by tensile tests. η and $\bar{\theta}$ can be calibrated depending on the shape of the specimens used in the fracture tests. In order to employ the M-C criterion in predicting failure, c_1 and c_2 should be determined by tests.

3. Modified M-C Criterion Parameter Calibration Approach

In order to calibrate the parameters of the M-C criterion, experimental tests and numerical simulations were conducted and the data were compared. The procedure is briefly described as follows:

- (a) Conduct a series of tests and obtain force–displacement responses.
- (b) Conduct parallel numerical simulations.
- (c) Determine the equivalent strain to fracture $\bar{\varepsilon}_f$ and stress triaxiality for each case from the test location of fracture initiation.
- (d) Plot the results from step c in the space of $(\bar{\varepsilon}_f, \eta, \bar{\theta})$ and construct the limiting fracture curve.

3.1. Experimental Tests

The aim of our tests was to obtain the material mechanical properties as well as the failure performance in different stress conditions. The parameters in Equation (12) were also calibrated by experimental data.

TC4 ELI is a kind of $\alpha + \beta$ titanium alloy containing approximately 6% aluminum and 4% vanadium. The TC4 ELI considered in this research is mill-annealed. Uni-axial tensile tests were firstly conducted to obtain the stress–strain curve and material mechanical properties. The specimen used for the uni-axial tensile tests is shown in Figure 2. The specimen mounted in the testing machine is shown in Figure 3. The fractography image is shown in Figure 4. The true stress–true strain curve is shown in Figure 5, and the mechanical properties are shown in Table 1.

In Table 1, R_p is the yield strength, R_m is the ultimate strength, and E is the Young's modulus.

After fitting the true stress–true strain curve to the power type flowing model, A and n are obtained, which are 1384 MPa and 0.082, respectively.

In order to investigate the ductile fracture behavior of TC4 ELI, as well as to obtain c_1 and c_2 , four kinds of specimens were designed inspired by Dara et al. [23,24]. Loads were applied to these specimens in different directions to obtain their fracture performance under different stress states. These stress states cover the negative-to-positive stress triaxiality and normalized Lode angle. Figure 6a shows the in-plane shear specimen used to study the failure behavior under a pure shear stress state. Figure 6b shows the multi-loading specimen which was subjected to tension combined with shear. Figure 6c,d show the failure behavior under the compression stress state with/without a notched gauge. A batch of four specimens was fabricated under the same conditions for each type of specimen to avoid material heterogeneity.

Table 1. Mechanical properties of TCE ELI.

R_p (MPa)	R_m (MPa)	E (GPa)	A (MPa)	n
770	952	108	1384	0.082

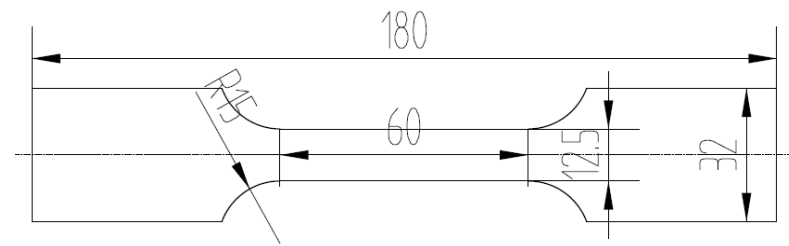


Figure 2. Specimen for uni-axial tensile tests (unit: mm).

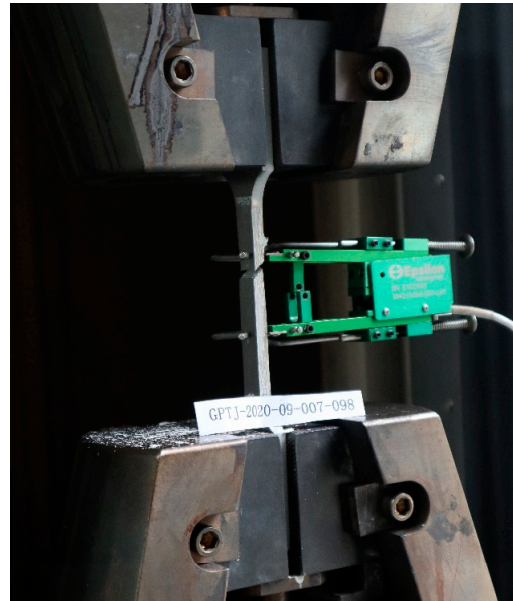


Figure 3. Tensile specimen mounted in the testing machine.

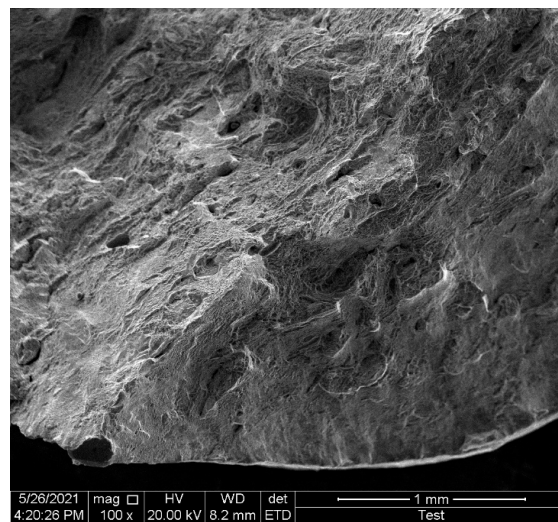


Figure 4. Tensile specimen fractography.

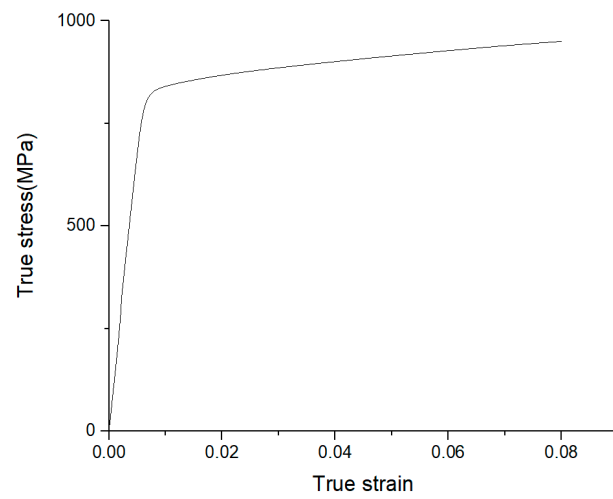


Figure 5. True stress–true strain of TC4 ELI.

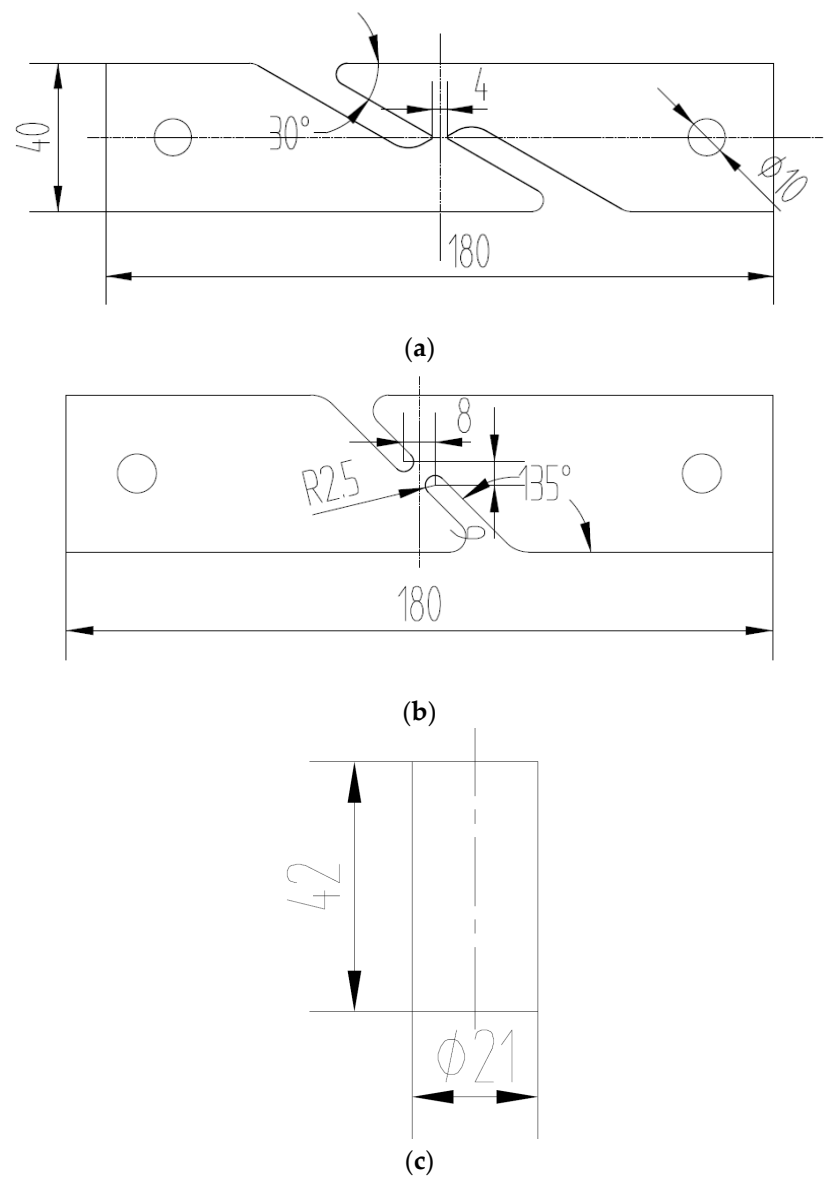


Figure 6. Cont.

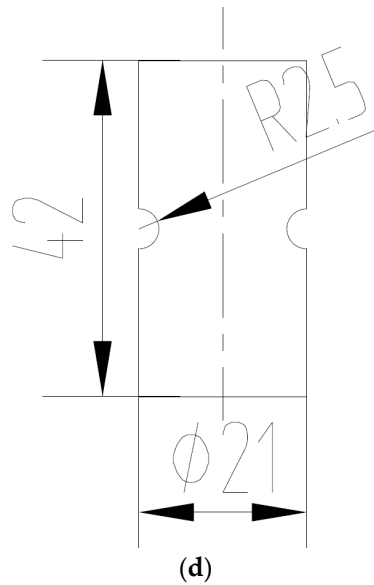


Figure 6. Illustration of specimens with dimensions (unit: mm). (a) In-plane shear specimen; (b) combined tension and shear specimen; (c) compression specimen without gauge; (d) compression specimen with gauge.

The specimens shown in Figure 6 were all strained until fracture using an INSTRON 8801 material testing machine (INSTRON, Shanghai, China), whose dynamic load capacity is ± 100 kN. A Digital Image Correlation (DIC) system was employed to obtain the failure process during loading.

Thanks to the variation in the stress conditions during loading in the experiments, the average stress triaxiality was computed to obtain an equivalent stress triaxiality value that summarized the experimental test conditions.

$$\eta_{av} = \frac{1}{\varepsilon_f} \int_0^{\bar{\varepsilon}_f} \eta d\varepsilon_{pe} \quad (13)$$

After the tests, the complete force versus displacement was recorded and material calibrations using the numerical simulations were based on these data to obtain the effective plastic strain failure.

3.2. Numerical Simulations and Parameter Calibration

For each kind of specimen geometry, a finite element model was established to simulate each experimental test. It was possible to reliably obtain the stress and strain states during the test and to achieve the failure calibration.

The finite element models were created using Abaqus/Explicit v6.14-1. In order to obtain the true performance of the stress–strain of specimens, the simulation models evaluated only the specimen geometry outside the clamping system. The areas at the end of the specimen model were constrained to reference points to control the moving behavior, applying the force on the reference point. One end of the specimens was set as fixed, the movement of other end of the specimens is set as 1.5 mm/s in the loading direction. The moving end of the specimens continued until the displacement was the same as that in the experiments. Linear bricks with reduced integration finite elements (C3D8R) were used in the models. The mesh control method was structured by cutting the specimens into several regular parts in advance. The element type was hexahedron or hexahedron-dominated. Inspired by Dara et al. [25,26], the regions where necking or failure may occur were finely meshed in order to obtain a compromise between calculation time and the ability to correctly describe the plastic strain. The element size was $0.2 \times 0.2 \times 0.2$ mm,

while the other part of the specimen was $2 \times 2 \times 2$ mm. The meshing density of the necking zone was ten times that of the other part. Figure 7 shows one example of the simulation models simulating pure shearing.

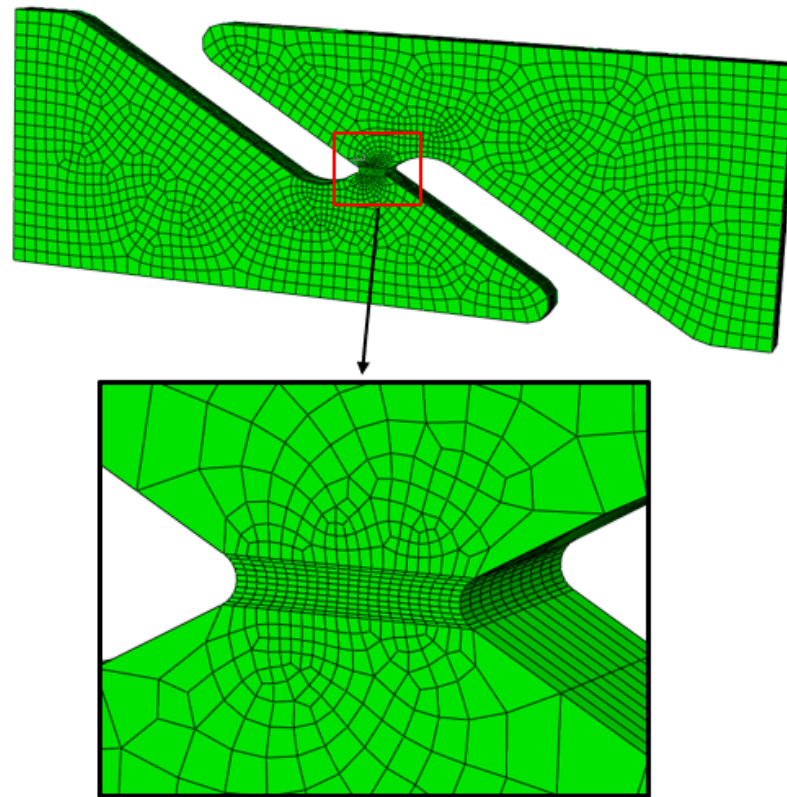


Figure 7. Simulation model of the specimen under pure shearing.

With the loading in the simulation models, the average stress triaxiality, the normalized Lode angle, and the effective plastic strain were calculated or simulated with the help of the user subroutine and software package.

After comparing the results of the tests and simulations, the effective plastic strains to failure of each case were determined, as shown in Table 2.

Table 2. Stress triaxiality, normalized Lode angle, and effective plastic strains to failure of the specimens under different stress state.

Specimen Type	η	$\bar{\theta}$	$\bar{\epsilon}_f$
Plastic plane strain, tension	0.333	1	0.6934
Pure shear	−0.0542	−0.0939	0.2424
Tension combined with shear	0.1251	0.3486	0.2951
Non-notched round bars, compression	−0.2780	−0.8215	0.8446
Notched round bars, compression (R2.5)	−0.8925	−1	1.7435

3.3. Determination of Parameters of M-C Criterion

With the help of the parameters A and n and the results in Table 2, the parameters c_1 and c_2 can be obtained by substituting the data of Table 2 into Equation (12). After the data fitting, the parameters of the modified M-C model were $c_1 = 0.0087$ and $c_2 = 711$ MPa. Using A , n , c_1 , and c_2 , the geometrical representation of the fracture locus based on the modified M-C model is given as in Figure 8.

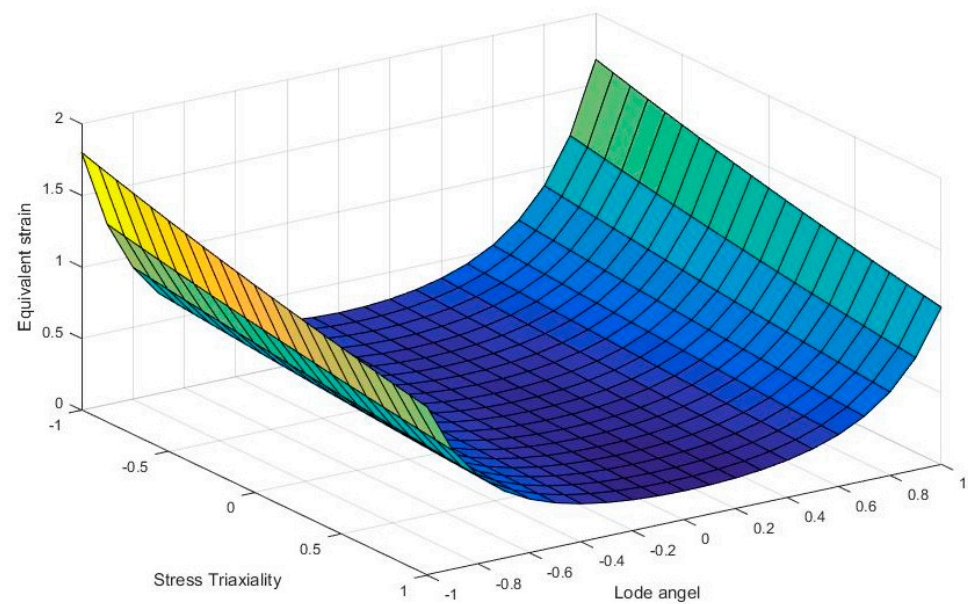


Figure 8. Three-dimensional geometric representation of modified Mohr–Coulomb fracture locus for TC4 ELI. (The warmer the tonality is, the higher the effective plastic strain to failure is. The colder the tonality is, the lower the effective plastic strain to failure is).

In order to verify the effectiveness of the model, the modified M-C model was embedded in the models mentioned in Section 3.2 to simulate the fracture of specimens under different loading states in Figure 4. The forces at fracture obtained by simulating are compared with those obtained in experiments mentioned in Section 3.1, as shown in Table 3.

Table 3. Comparison of the forces at fracture between simulations and experiments.

Specimen Type	Force at Fracture in Test (kN)	Force at Fracture in Simulation (kN)	Error
Plastic plane strain, tension	57.7	55.1	−4.5%
Pure shear	13.8	14.1	+2.2%
Tension combined shear	18.1	19.0	+5.0%
Non-notched round bars, compression	563.2	591.4	+5.0%
Notched round bars, compression (R2.5)	407.4	425.3	+4.4%

After comparing the forces at fracture between the simulations and experiments, it was shown that the errors of the forces of simulations were all below 5%, which proved the effectiveness of the modified M-C model in simulations of the fracture behavior under the stress states mentioned in Section 3.1.

4. Application

In order to apply the modified M-C fracture criterion in predicting the ultimate strength of pressure hulls under external pressure, a ring-stiffened cylinder was designed. The cylinder was fine-machined in order to avoid the influence of plastic deformation. The cylinder was made of TC4 ELI, which is shown in Figure 9. The inner diameter of the cylinder was 200 mm, with a thickness of 8 mm. The length of the cylinder was 300 mm, with the height of the ring being 40 mm.



Figure 9. Fine-machined, ring-stiffened cylinder (TC4 ELI).

External pressure was applied to the cylinder until fracture. The ultimate strength of the cylinder was 31.5 MPa according to the measurements during the experiment. Thanks to the properties of titanium alloy, which has a low toughness and high yield-to-tensile ratio, the fractured cylinder was fragmented. The cylinder after the external pressure experiment is shown in Figure 10.



Figure 10. The cylinder after the external pressure experiment.

The simulation of the cylinder under external pressure was performed in Abaqus with the help of the modified M-C model. The dimensions of the cylinder in the simulation were the same as those in the experiment. Linear bricks with reduced integration finite elements (C3D8R) were used in the models and the mesh control method was also structured. The element type was a hexahedron. The element size was $2 \times 2 \times 2$ mm. The modified M-C criterion and the parameters were embedded in Abaqus with the help of the user subroutine VUSDFLD. The external pressure was applied on all outer surfaces of the cylinder, and

it was increased in increments of 0.5 MPa until fracture. The simulation model of the ring-stiffened cylinder is shown in Figure 11.

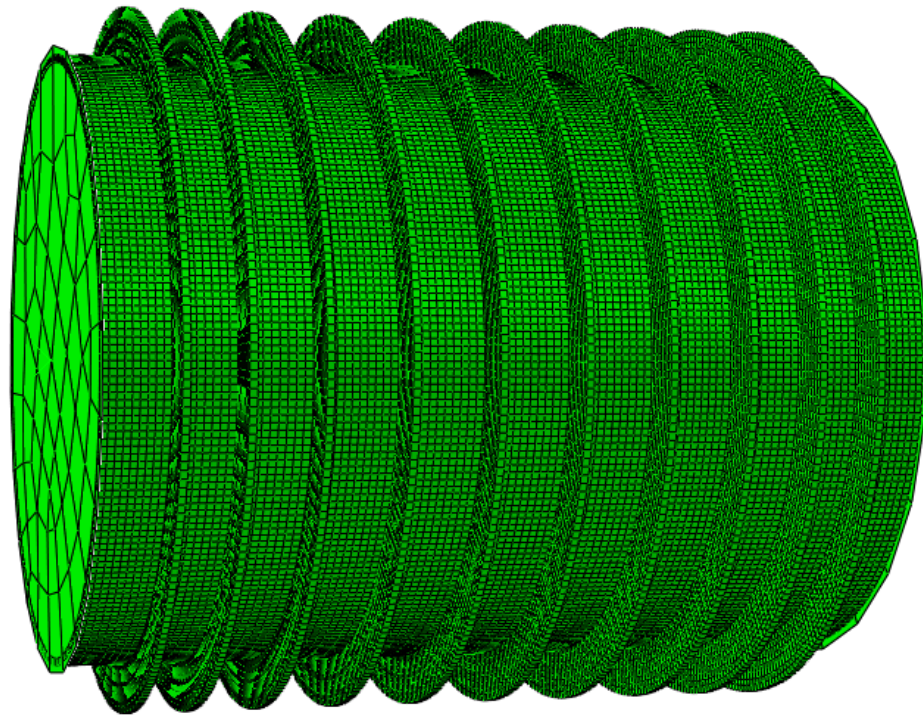


Figure 11. The simulation model of the ring-stiffened cylinder.

After the loading, the fractured cylinder was as shown in Figure 12, which was also fragmented. The ultimate strength of the cylinder in simulation with modified M-C criterion was 33.5 MPa, with the error 6.35%.

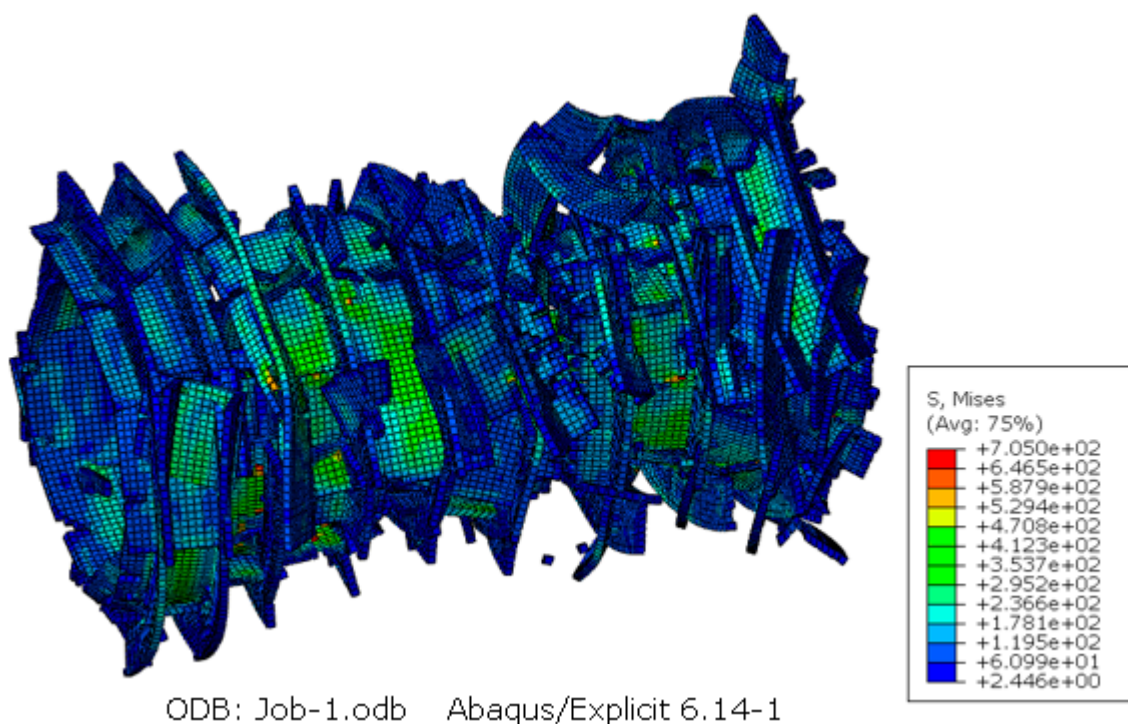


Figure 12. The fracture state of the cylinder in the simulation.

5. Discussion

The original M-C criterion was established for cracks in rock and soil mechanics and other brittle materials. The cracking behavior of titanium alloy is similar to that of brittle materials because of its low toughness and high yield-to-tensile ratio. This phenomenon can allow authors to apply the M-C model to predict the cracking of titanium alloy.

The pressure hull made of titanium alloy in this paper was assumed to suffer external pressure from working in a deep-sea environment. So, more compression testing specimens were designed to obtain the parameters of the modified M-C model and the fracture locus in the form of $\bar{\epsilon}_f, \eta, \bar{\theta}$. If the modified M-C model is employed to predict fractures of other stress states, specimens with different shapes should be designed in order to obtain more accurate parameters.

The result of the simulation in Section 4 was a little higher than that in our experiment. This is because there were still tiny imperfections on the cylinder made by fine machining. However, the cylinder in the simulation model was assumed to be perfect.

6. Conclusions

In order to investigate the fracture behavior of titanium alloy, which is widely used in the field of ocean engineering, the classical Mohr–Coulomb fracture criterion was modified to predict cracking occurring on a ring-stiffened cylinder suffering external pressure in this paper. The parameters of the modified M-C criterion were calibrated based on five kinds of specimens under different stress states and the ultimate strength of the ring-stiffened cylinder made of TC4 ELI predicted by the modified M-C criterion was close to the results obtained in our experiment, which shows that the modified M-C criterion is suitable for use in cracking predictions of titanium alloy. It is an effective method for investigating the ultimate strength of pressure hulls made of titanium alloy used in the deep-sea field.

In future work, the anisotropic nature of titanium alloys should be considered in the modified M-C criterion, and sensitivity analyses should also be conducted to determine the robustness of the simulation results. It is also necessary to compare the M-C criterion with traditional and advanced prediction methods in future.

Author Contributions: Conceptualization, X.Y.; methodology, X.Y.; software, X.Y. and H.Z.; validation, K.X.; investigation, X.Y.; data curation, X.Y.; writing—original draft preparation, X.Y.; writing—review and editing, Q.X.; project administration, Q.X. and A.Z. All authors have read and agreed to the published version of the manuscript.

Funding: This research received no external funding.

Data Availability Statement: The experimental and raw simulation results cannot be shared at this time because further analysis is required for ongoing work.

Conflicts of Interest: The authors declare no conflict of interest.

References

1. Gurson, A.L. Continuum Theory of Ductile Rupture by Void Nucleation and Growth—1. Yield Criteria and Flow Rules for Porous Ductile Media. *J. Eng. Mater. Technol.* **1977**, *99*, 2–15. [[CrossRef](#)]
2. Tvergaard, V. On localization in ductile materials containing spherical voids. *Int. J. Fract.* **1982**, *18*, 237–252. [[CrossRef](#)]
3. Needleman, A.; Tvergaard, V. Analysis of ductile rupture in notched bars. *J. Mech. Phys. Solids* **1984**, *32*, 461–490. [[CrossRef](#)]
4. Nahshon, K.; Hutchinson, J.W. Modification of the Gurson Model for shear failure. *Eur. J. Mech. A Solids* **2008**, *27*, 1–17. [[CrossRef](#)]
5. Nielsen, K.L.; Tvergaard, V. Ductile shear failure or plug failure of spot welds modelled by modified Gurson model. *Eng. Fract. Mech.* **2010**, *77*, 1031–1047. [[CrossRef](#)]
6. Xue, L. Constitutive modeling of void shearing effect in ductile fracture of porous materials. *Eng. Fract. Mech.* **2008**, *75*, 3343–3366. [[CrossRef](#)]
7. Lemaitre, J. Continuous damage mechanics model for ductile fracture. *J. Eng. Mater. Technol. Trans. ASME* **1985**, *107*, 83–89. [[CrossRef](#)]
8. Chaboche, J.L. Continuum Damage Mechanics: Part I—General Concepts. *J. Appl. Mech.* **1988**, *55*, 59–64. [[CrossRef](#)]
9. Chaboche, J.L. Continuum Damage Mechanics: Part II—Damage Growth, Crack Initiation, and Crack Growth. *J. Appl. Mech.* **1988**, *55*, 65–72. [[CrossRef](#)]

10. Brünig, M. Continuum framework for the rate-dependent behavior of anisotropically damaged ductile metals. *Acta Mech.* **2006**, *186*, 37. [[CrossRef](#)]
11. McClintock, F.A.; Kaplan, S.M.; Berg, C.A. Ductile fracture by hole growth in shear bands. *Int. J. Fract.* **1966**, *2*, 614–627. [[CrossRef](#)]
12. Cockcroft, M.G.; Latham, D.J. Ductility and the workability of metals. *J. Inst. Met.* **1968**, *96*, 33–39.
13. Rice, J.R.; Tracey, D.M. On ductile enlargement of voids in triaxial stress fields. *J. Mech. Phys. Solids* **1969**, *17*, 201–217. [[CrossRef](#)]
14. Brozzo, P.; Deluca, B.; Rendina, R. *A New Method for the Prediction of Formability in Metal Sheets*; IDDRG: Amsterdam, The Netherlands, 1972.
15. Oyane, M.; Sato, T.; Okimoto, K.; Shima, S. Criteria for ductile fracture and their applications. *J. Mech. Work. Technol.* **1980**, *4*, 65–81. [[CrossRef](#)]
16. Cliff, S.E.; Hartley, P.; Sturgess, C.E.N.; Rowe, G.W. Fracture prediction in plastic deformation processes. *Int. J. Mech. Sci.* **1990**, *32*, 1–17. [[CrossRef](#)]
17. Ko, Y.K.; Lee, J.S.; Huh, H.; Kim, H.K.; Park, S.H. Prediction of fracture in hub-hole expanding process using a new ductile fracture criterion. *J. Mater. Process. Technol.* **2007**, *187*, 358–362. [[CrossRef](#)]
18. Bai, Y.; Wierzbicki, T. A new model of metal plasticity and fracture with pressure and Lode dependence. *Int. J. Plast.* **2008**, *24*, 1071–1096. [[CrossRef](#)]
19. Bai, Y.; Wierzbicki, T. Application of extended Mohr-Coulomb criterion to ductile fracture. *Int. J. Fract.* **2010**, *161*, 1–20. [[CrossRef](#)]
20. Liang, X. Damage accumulation and fracture initiation in uncracked ductile solids subject to triaxial loading. *Int. J. Solids Struct.* **2007**, *44*, 5163–5181.
21. Khan, A.S.; Liu, H. A new approach for ductile fracture prediction on Al 2024-T351 alloy. *Int. J. Plast.* **2012**, *35*, 1–12. [[CrossRef](#)]
22. Isik, K.; Silva, M.B.; Tekkaya, A.E.; Martins, P.A.F. Formability limits by fracture in sheet metal forming. *J. Mater. Process. Technol.* **2014**, *214*, 1557–1565. [[CrossRef](#)]
23. Dara, A.; Johnney Mertens, A.; Raju Bahubalendruni, M.V.A. Characterization of penetrate and interpenetrate tessellated cellular lattice structures for energy absorption. *Proc. Inst. Mech. Eng. Part L J. Mater. Des. Appl.* **2023**, *237*, 906–913. [[CrossRef](#)]
24. Dara, A.; Bahubalendruni, M.R.; Mhaskar, A.; Choudhary, V.; Balamurali, G.; Turaka, S. Experimental and numerical investigation on 2.5-dimensional nature-inspired infill structures under out-plane quasi-static loading. *Proc. Inst. Mech. Eng. Part E J. Process Mech. Eng.* **2023**, *237*, 906–913.
25. Dara, A.; Bahubalendruni, M.A.R.; Mertens, A.J.; Balamurali, G. Numerical and experimental investigations of novel nature inspired open lattice cellular structures for enhanced stiffness and specific energy absorption. *Mater. Today Commun.* **2022**, *31*, 103286. [[CrossRef](#)]
26. Dara, A.; Raju Bahubalendruni, M.V.A.; Johnney Mertens, A.; Balamurali, G. A novel nature inspired 3D open lattice structure for specific energy absorption. *Proc. Inst. Mech. Eng. Part E J. Process Mech. Eng.* **2022**, *236*, 2434–2440.

Disclaimer/Publisher’s Note: The statements, opinions and data contained in all publications are solely those of the individual author(s) and contributor(s) and not of MDPI and/or the editor(s). MDPI and/or the editor(s) disclaim responsibility for any injury to people or property resulting from any ideas, methods, instructions or products referred to in the content.